Visualizing the Analogy between Competitive Adsorption and Colloid Stability to Restore Lung Surfactant Function

Ian C. Shieh,[†] Alan J. Waring,[‡] and Joseph A. Zasadzinski[§*]
[†]Department of Chemical Engineering, University of California, Santa Barbara, California; [‡]Department of Medicine, David Geffen School of Medicine, University of California, Los Angeles, California; and [§]Department of Chemical Engineering and Materials Science, University of Minnesota, Minneapolis, Minnesota

ABSTRACT We investigated a model of acute respiratory distress syndrome in which the serum protein albumin adsorbs to an air-liquid interface and prevents the thermodynamically preferable adsorption of the clinical lung surfactant Survanta by inducing steric and electrostatic energy barriers analogous to those that prevent colloidal aggregation. Chitosan and polyethylene glycol (PEG), two polymers that traditionally have been used to aggregate colloids, both allow Survanta to quantitatively displace albumin from the interface, but through two distinct mechanisms. Direct visualization with confocal microscopy shows that the polycation chitosan coadsorbs to interfacial layers of both Survanta and albumin, and also colocalizes with the anionic domains of Survanta at the air-liquid interface, consistent with it eliminating the electrostatic repulsion by neutralizing the surface charges on albumin and Survanta. In contrast, the PEG distribution does not change during the displacement of albumin by Survanta, consistent with PEG inducing a depletion attraction sufficient to overcome the repulsive energy barrier toward adsorption.

INTRODUCTION

Lung surfactant (LS) is a mixture of lipids and proteins that lowers the surface tension at the air-liquid interface of the epithelial fluid in the millions of alveoli in the lungs. LS allows for proper respiration by minimizing the work of inhalation and preventing alveolar collapse upon exhalation (1). A disruption in the normal function of LS contributes to acute respiratory distress syndrome (ARDS), which is characterized by a rapid onset of respiratory failure (2) and affects 150,000 people annually in the United States with 40% mortality (2–4). Although the pathogenesis of ARDS is not fully understood, a contributing factor is the inactivation of LS by serum proteins, such as albumin, that leak into the lungs as a result of increased permeability of the alveolar capillaries caused by another underlying disease or trauma (2,4,5). Concentrations of albumin and other serum proteins in the alveolar fluid are elevated during ARDS (6), and an ARDS-like decrease in LS performance occurs both in animal models (5) and in vitro when serum proteins are present at these abnormally high concentrations (4,7–10).

Many serum proteins are surface active and thus compete with LS to occupy the alveolar air-liquid interface (7–9,11), but do not sufficiently reduce surface tension in the lungs for respiration. Albumin, the most prevalent serum protein, spontaneously adsorbs to the air-liquid interface and increases the surface pressure to (i.e., reduces the surface tension by) 20–25 mN/m (7,9). Because albumin is soluble in the alveolar fluid, interfacial albumin molecules desorb during exhalation as the interfacial area decreases, and the remaining molecules on the interface do not pack tightly enough to reach the high surface pressures necessary for respiration (4,7–10). In comparison, LS adsorbs to an equilibrium surface pressure of 45–50 mN/m (8) and does not desorb from the interface with decreasing surface area. Therefore, LS forms a tightly packed interfacial monolayer that achieves a maximum surface pressure of 65–70 mN/m (sufficient for respiration) due to collapse of the monolayer (12) rather than desorption of surfactant from the interface.

Equilibrium thermodynamics predicts that a LS film should always displace an albumin film at an air-liquid interface because LS lowers the surface energy more than albumin (by 45–50 versus 20–25 mJ/m^2) (9). However, this thermodynamically favorable replacement is kinetically limited and may not occur for hours or more (4,8,9,13,14). Albumin (diameter ~10 nm) diffuses ~1000-fold faster than the larger LS aggregates (diameter ~10 μm) because the diffusion coefficient for spherical particles is inversely proportional to diameter. As a result, albumin reaches the newly created air-liquid interface more rapidly than LS during inhalation. Once at the interface, the negatively charged albumin (15) induces a repulsive energy barrier (16–18) that prevents LS, which is also negatively charged (19), from reaching the interface (Fig. 1 *A*). This kinetically hindered equilibrium shares many features with the Derjaguin-Landau-Verwey-Overbeek (DLVO) theory of colloid stability (9,16–18). Colloidal dispersions do not reach equilibrium (i.e., aggregate) for years if the energy barrier toward aggregation is sufficiently high.

Oppositely charged polyelectrolytes promote aggregation of charged colloids and also enhance surfactant adsorption in the presence of albumin and other serum proteins by reducing electrostatic repulsions (20,21). The DLVO

Submitted July 20, 2011, and accepted for publication January 9, 2012.

*Correspondence: zasad008@umn.edu

Editor: William Wimley.

0006-3495/12/02/0777/10 $2.00

doi: 10.1016/j.bpj.2012.01.014

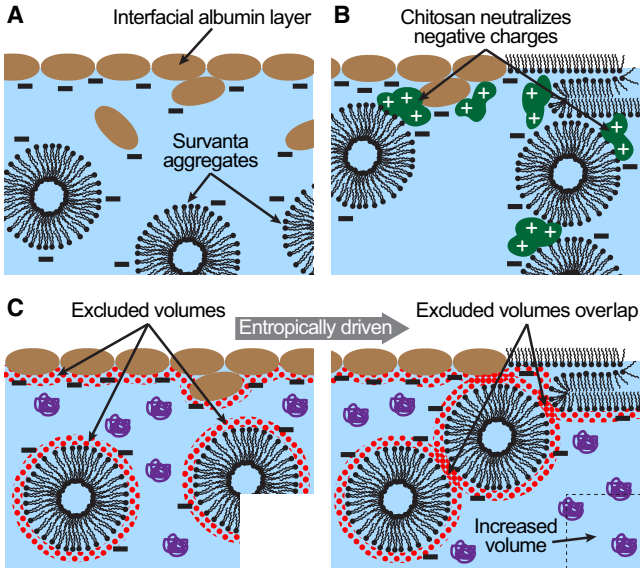

FIGURE 1 Schematic diagrams of albumin inhibition of the clinical LS Survanta and two distinct mechanisms of polymer-enhanced Survanta adsorption. (*A*) Albumin-inhibited diffusion of Survanta to the interface. The negative charges on albumin and Survanta create an electrostatic barrier that prevents Survanta from reaching the interface (Eq. 1). (*B*) Polycationic chitosan binds to the negative charges on albumin and Survanta, and reduces the magnitude of the electrostatic barrier toward Survanta diffusion to the interface, which allows Survanta to replace the interfacial film of albumin. (*C*) PEG is physically excluded from approaching the interface, albumin, or Survanta aggregates within the radius of gyration of PEG (*dotted regions*). When these excluded volumes overlap, PEG cannot enter the gap between the Survanta aggregates and the interface (or between aggregates), which leads to an osmotic pressure that pushes the aggregates toward the interface or each other. This is equivalent to increasing the volume available to PEG, which is an entropically favorable process (Eq. 2).

potential combines repulsive double-layer electrostatic forces with attractive van der Waals interactions to explain the stability of charged colloidal suspensions and the inhibition of LS adsorption by albumin. Between two spheres of radius, a, at separation, r, surface potential, ψ_s, bulk ion concentration, n_i, of valence, z_i, and Debye length, $\kappa^{-1} = \sqrt{(\varepsilon\varepsilon_0 kT)/(e^2\sum_i z_i^2 n_i)}$, the DLVO potential, Φ_{DLVO}, is (18):

$$\Phi_{DLVO} = 32\pi\varepsilon\varepsilon_0\left(\frac{kT}{ez}\right)^2 a\tanh^2\left(\frac{ez\psi_s}{4kT}\right) \times \exp(-\kappa(r-2a)) - \frac{aA_H}{12(r-2a)}, \quad (1)$$

where A_H is the Hamaker constant that determines the magnitude of the attractive forces, ε is the dielectric constant, ε_0 is the vacuum permittivity, e is the elementary charge, k is the Boltzmann constant, T is the absolute temperature, and z is the valency of the electrolyte counterions. The surface potential, ψ_s, affects the magnitude of the repulsive electrostatic forces and is proportional to the surface charge density, σ, of albumin or LS (16–18). The surface charge density is set by the pK values of the amino acids in albumin or the charged lipids in LS (both albumin and LS are negatively charged at neutral pH). The extent of dissociation of the charged surface groups of albumin and LS also depends on the pH and total electrolyte concentration of the subphase liquid (22). The linear and polycationic polysaccharide chitosan (20,21,23,24) reduces σ, and hence ψ_s, by binding to the anionic groups on albumin and/or LS, which reduces the electrostatic repulsion and lowers the energy barrier toward LS adsorption (Fig. 1 *B*).

Rather than reducing the electrostatic repulsion between colloids (or albumin and LS), nonadsorbing polymers induce an attractive interaction that can cause colloidal aggregation or adsorption of LS. Polyethylene glycol (PEG) and dextran increase adsorption of LS to an albumin-covered air-liquid interface (8,13,25–27) and improve oxygenation in animals with lung injuries when added to LS (28–30). These neutral polymers do not change the surface charge density, surface potential, or Debye length in Eq. 1, but instead induce a depletion-attraction potential that reduces the net repulsive potential. If LS particles of radius, a, immersed in a polymer solution of volume fraction, ϕ_p, approach the interface more closely than the effective polymer diameter, 2 R_g, the polymer can no longer fit into the excluded volume between the sphere and the interface (14,31,32). The polymer concentration is reduced in the excluded volume, resulting in a lower osmotic pressure. Consequently, the osmotic pressure on the large sphere becomes unbalanced, leading to a depletion-attraction force that pushes the LS particle toward the interface (14,31,32):

$$\Phi_{dep} = -3\phi_p kT\frac{a}{R_g}\left(1-\frac{r}{2R_g}\right)^2. \quad (2)$$

Simply adding Φ_{dep} to Φ_{DLVO} in Eq. 1 to account for the presence of nonadsorbing polymers in solution reduces the net repulsive potential and promotes LS adsorption (Fig. 1 *C*). However, to induce a depletion attraction, the polymer must remain homogeneously distributed in solution and not adsorb to the interface, LS, or albumin.

The two distinct mechanisms of electrostatic neutralization and depletion attraction for promoting LS adsorption in the presence of an inhibitory interfacial albumin film result in two distinct polymer distributions. Here, we used confocal fluorescence microscopy to determine the three-dimensional distributions of fluorescently labeled LS, albumin, chitosan, and PEG in the vicinity of the air-liquid interface. We present evidence that 1), an albumin film prevents the clinical LS Survanta from adsorbing to the air-liquid interface; 2), the polycation chitosan adsorbs to both albumin and Survanta, decreases their surface charges and electrostatic repulsion, and thereby promotes the quantitative exchange of albumin with Survanta at the interface; and 3) the neutral, hydrophilic PEG also promotes

exchange of albumin with Survanta, but through an attractive depletion-attraction mechanism in which the distribution of PEG in solution and at the interface does not change.

MATERIALS AND METHODS

Surfactants and subphase

Bovine serum albumin, PEG (10 kDa), and 75–85% deacetylated chitosan (50–190 kDa) were obtained from Sigma-Aldrich (St. Louis, MO). Chitosan is a linear polysaccharide composed of units of *N*-acetyl-D-glucosamine and its deacetylated counterpart, D-glucosamine, whose amino groups become protonated under neutral to acidic conditions. A Milli-Q Gradient A10 system (Millipore, Billerica, MA) provided ultrapure water with a resistivity of at least 18.0 MΩ·cm. MOPS-buffered saline (150 mM NaCl, 2 mM $CaCl_2$, 1 mM 3-(*N*-morpholino)propanesulfonic acid, pH 7.0) was used to prepare the aqueous subphase. Albumin and PEG were prepared as stock solutions in the MOPS-buffered saline, and the chitosan was dissolved in 150 mM NaCl with 1% acetic acid. Bovine serum albumin labeled with Texas Red (TR-albumin; Invitrogen, Carlsbad, CA) and 10-kDa PEG conjugated to fluorescein isothiocyanate (FITC-PEG; Nanocs, New York, NY) were prepared as solutions in 150 mM NaCl. Dipalmitoylphosphatidylethanolamine with Texas Red (TR-DPPE) conjugated to the headgroup was purchased from Invitrogen. Survanta (Abbott Nutrition, Columbus, OH) was generously provided by the Santa Barbara Cottage Hospital neonatal intensive care unit. Survanta, a clinically used replacement LS, is an organic extract of minced bovine lungs fortified with dipalmitoylphosphatidylcholine (DPPC), palmitic acid, and tripalmitin. We prepared samples of Survanta by diluting it from 25 mg/mL to 2 mg/mL in 150 mM NaCl. Each sample was sonicated for 30 s to ensure proper mixing and to break up flocculates, and stored at 4°C. Before use, the diluted Survanta was returned to room temperature and vortexed. Immediately before each experiment, we premixed a fresh 120 mL subphase in glass using the appropriate stock solutions and MOPS-buffered saline. Subphases containing chitosan were adjusted to pH 6.8–7.0 with 1 M NaOH. A total of 1 mg of Survanta and subphase concentrations of 2 mg/mL albumin, 25 μg/mL chitosan, and 30 mg/mL PEG were used in this work unless otherwise noted.

Fluorescently labeled chitosan

Chitosan was fluorescently labeled (AF-chitosan) with Alexa Fluor 488 carboxylic acid succinimidyl ester (Invitrogen). The chitosan was incubated in 10 mM sodium acetate buffer (pH 7.0) with the fluorescent dye added in dimethyl formamide at a volume ratio of 1:20 (dimethyl formamide/buffer) to a final molar ratio of 1:1 (dye/chitosan). The mixture was incubated at 37°C with shaking for 2 h, followed by dialysis of the sample for 48 h against 10 mM HCl to remove unbound dye. The degree of chitosan labeling was found to be ~1:120 (mol dye/mol chitosan) as estimated by gravimetric analysis and absorption spectroscopy of the dye conjugate at 495 nm in 200 mM sodium acetate buffer (pH 2.7) assuming a molar extinction coefficient of 71,000 $cm^{-1}\cdot M^{-1}$ (33). An average molecular mass for chitosan of 120 kDa was used for all calculations.

Surface balance measurements

We performed experiments using a custom-milled Teflon Langmuir trough with continuous steel ribbon barriers. We measured surface pressure (i.e., the reduction in surface tension of a clean air-water interface, 72 mN/m at 25°C) using a filter paper Wilhelmy plate tensiometer (Riegler and Kirstein, Germany). Interfacial temperature was measured with a miniature infrared thermocouple (Omega Engineering, Stamford, CT) and controlled at 25°C via a circulating water bath. All experiments were conducted at 25°C, rather than 37°C, to reduce convection and evaporation that disrupted image acquisition. Although this is below physiological temperature, the phase behavior of Survanta remains similar over the range of 20–37°C (34). Additionally, both the DLVO potential (Eq. 1) and the depletion attraction (Eq. 2) do not change significantly over this temperature range (18). A custom-milled Delrin cover limited evaporation to negligible levels. A custom computer interface written in LabVIEW 9.0 (National Instruments, Austin, TX) handled all aspects of trough control and data collection.

We deposited the aqueous Survanta suspension into the Langmuir trough dropwise by using a glass microsyringe and touching each drop to the air-liquid interface. Although some of the Survanta was immediately deposited on the interface, most of it went into the aqueous subphase and then adsorbed to the interface. After a 20-min period to allow for this adsorption to occur, the trough was cycled eight times from a maximum area of 145 cm^2 to a minimum area of 50 cm^2 at a rate of 20 cm^2/min.

Laser scanning confocal fluorescence microscopy

We used a C1 confocal scan head fitted on a Nikon Eclipse 80i upright microscope (Nikon Instruments, Melville, NY) with a Nikon plan apochromatic 20× air immersion objective with a working distance of 1 mm, 0.75 NA, and correction for a 170 μm glass coverslip. A 12-mm-diameter, 170-μm-thick, round glass coverslip was attached to the tip of the objective to minimize spherical aberration due to refractive index mismatch (35). The objective was resistively heated to 35°C to minimize condensation. Fluorescence contrast was provided by small amounts of dye-conjugated components. Concentrations of 5 μg/mL AF-chitosan, 15 μg/mL FITC-PEG, and 10 μg/mL TR-albumin were added with appropriate amounts of the unlabeled species during subphase preparation. Survanta samples were doped with 1 wt% TR-DPPE (as a suspension in ultrapure water) during dilution and before sonication.

At a given surface pressure or surface area, the trough barriers were paused and a series (z-stack) of images was acquired from 7 μm above to 10 μm below the air-liquid interface at 0.5 μm intervals. The imaging plane was oriented parallel to the air-liquid interface in the Langmuir trough. Each image required ~1 s to raster scan across 512 × 512 pixels representing 150 × 150 μm. It took 40 s to acquire a complete z-stack, and the surface pressure remained effectively constant (±2 mN/m maximum deviation) during acquisition. The sample was excited by both 488 nm and 594 nm lasers to allow for simultaneous visualization of two fluorophores. We acquired the z-stacks starting at the second compression cycle after adding the subphase to the trough and/or starting at the fourth compression cycle after depositing Survanta into the subphase.

To characterize interfacial phenomena in the Langmuir trough, we used conventional images of the air-liquid interface extracted from the image stack as well as axial fluorescence intensity profiles calculated from the z-stack. To calculate an axial intensity profile, the pixel fluorescence intensity for each image slice was averaged, normalized to the maximum intensity of all slices in the z-stack, and plotted as a function of the axial position.

Deconvolution methodology

The measured signal in an optical system is the convolution of the microscope point-spread function (PSF) with the true image of the sample (35). To determine the PSF, we measured the axial fluorescence profile of a fluorescently labeled DPPC monolayer (see Fig. 3 *A*). The 3-nm-thick monolayer effectively represents a δ-function in fluorescence intensity; the convolution between the PSF and the δ-function equals the PSF, so the measured profile of the DPPC monolayer represents the microscope PSF. To form the monolayer, 20 μg of DPPC (Avanti Polar Lipids, Alabaster, AL) doped with 0.5 wt% TR-DPPE in a 2 mg/mL chloroform solution were spread dropwise onto a subphase of 120 mL of ultrapure

water at 25°C. Z-stacks were acquired at surface pressures ranging from 5 to 60 mN/m. The resulting fluorescence profiles were averaged and linearly interpolated at 10 nm intervals to determine the PSF for the optical system. We then convolved this experimentally acquired PSF with appropriate input models using a discrete convolution algorithm to best match the measured axial fluorescence profiles for Survanta, albumin, chitosan, and PEG.

Colocalization of material

We quantified the degree of lateral colocalization between red (i.e., Survanta) and green (i.e., chitosan or PEG) fluorescence using the Pearson's colocalization coefficient, r_p (35):

$$r_p = \frac{\sum_i \left[\left(R_i - R_{avg}\right)\left(G_i - G_{avg}\right)\right]}{\sqrt{\sum_i \left(R_i - R_{avg}\right)^2 \sum_i \left(G_i - G_{avg}\right)^2}}, \quad (3)$$

where R_i and G_i are the red and green intensities, respectively, of pixel i, and R_{avg} and G_{avg} are the red and green intensities, respectively, averaged over the whole image.

RESULTS

Reversing the albumin-induced inactivation of Survanta

Compression-expansion isotherms for Survanta deposited on a physiological saline subphase, with or without albumin, demonstrated normal (no albumin) and inhibited (with albumin) LS function (Fig. 2 *A*). In the absence of albumin, Survanta reached surface pressures > 65 mN/m when compressed to mimic the change in alveolar area upon exhalation. During expansion, the surface pressure decreased rapidly and demonstrated the characteristic hysteresis of normal LS (34). However, when Survanta was deposited on a subphase containing albumin to mimic ARDS-like conditions (4,6,9), the surface pressure did not increase during compression. Instead, the isotherm matched that of albumin alone. This indicates that Survanta did not reach the interface in sufficient quantity to substantially raise the surface pressure because of the electrostatic energy barrier toward adsorption induced by the interfacial albumin film (Fig. 1 *A*) (13).

Adding either chitosan (Fig. 2 *B*) or PEG (Fig. 2 *C*) to the subphase reversed the inhibitory effects of albumin. An optimal chitosan concentration of 25–50 μg/mL restored the maximum surface pressure to ~65 mN/m, whereas 100 μg/mL of chitosan was not as effective and the maximum surface pressure dropped. A substantially higher concentration of PEG (30 mg/mL) in the albumin-containing subphase restored the characteristic features of the Survanta isotherm, as indicated by the maximum surface pressure increasing to ~70 mN/m. The shift of the compression curve toward larger trough areas with increasing concentrations of PEG was consistent with increasing surface concentrations of Survanta (13). Of interest, the optimum concentration of chitosan was 1000-fold lower than that of PEG, and inhibition returned with higher than optimal amounts of chitosan. These observations suggest that chitosan neutralized the negative surface charges of albumin and Survanta (Fig. 1 *B* and Eq. 1) and then overcompensated for them, whereas the neutral PEG induced a depletion attraction proportional to the PEG volume fraction (Fig. 1 *C* and Eq. 2).

Axial fluorescence distributions

Three distinct axial fluorescence intensity profiles resulted from Survanta (Fig. 3 *B*), albumin (Fig. 3 *C*), and either chitosan or PEG (Fig. 3 *D*) as single components in the Langmuir trough. The measured fluorescence intensities (*symbols*) were fit (*solid curves*) to a convolution of the true fluorescence profiles (*dotted lines*) and the microscope PSF, as determined using a solvent-spread DPPC monolayer (Fig. 3 *A*) (35). The fluorescence intensity profile for Survanta had a Gaussian-like shape (Fig. 3 *B*), which was similar to but wider than that of the DPPC monolayer. The Survanta profile indicated a high concentration at the air-liquid interface and negligible concentration elsewhere, as expected for an insoluble, multilayered surfactant film (13,34) at the air-liquid interface. Albumin, a soluble surfactant, had an asymmetric fluorescence intensity profile (Fig. 3 *C*) consistent with a high interfacial concentration and a uniform subphase concentration. The albumin concentration

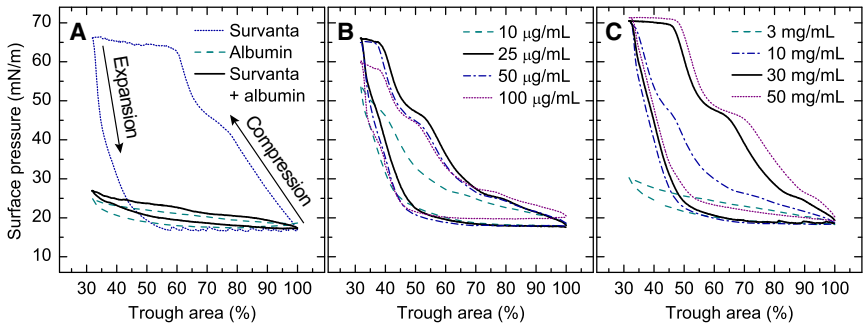

FIGURE 2 Third-cycle isotherms at 25°C demonstrate the normal, inhibited, and polymer-restored activity of Survanta. (*A*) Survanta (*dotted line*) deposited dropwise in a physiological, buffered-saline subphase. The maximum surface pressure was > 65 mN/m (surface tension < 10 mN/m) upon compression, with significant hysteresis upon expansion. For a subphase containing albumin (*dashed line*), there were minimal changes in surface pressure with changes in interfacial area, consistent with the expected desorption-adsorption behavior of the soluble, surface-active albumin. When Survanta was added to a subphase containing albumin (Survanta + albumin, *solid black line*), the isotherm nearly matched that of pure albumin. (*B*) Survanta added to subphases containing albumin and a series of chitosan concentrations. Increasing chitosan concentrations first restored the normal Survanta isotherm, but then caused less Survanta to adsorb and the maximum surface pressure to decrease. (*C*) Survanta added to subphases containing albumin and a series of PEG concentrations. Increasing the PEG concentration restored the normal Survanta isotherm.

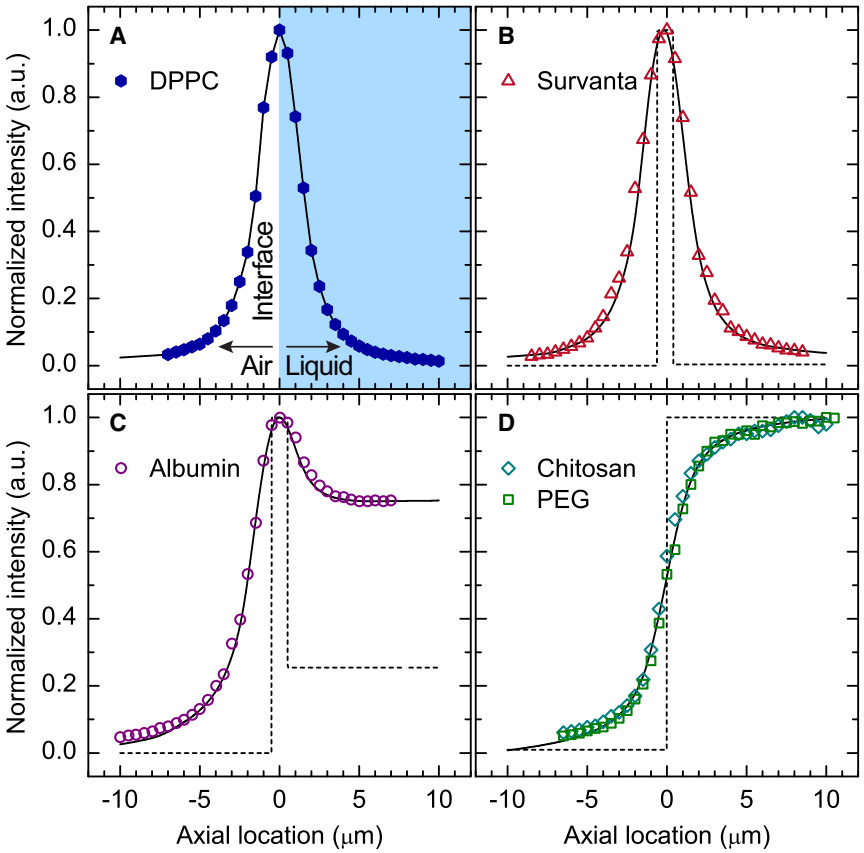

FIGURE 3 Axial fluorescence intensity profiles measured via confocal microscopy. (*A*) Solvent-spread DPPC monolayer at the air-water interface representing a δ-function in fluorescence intensity used to measure the microscope PSF. The solid lines in (*B–D*) represent the convolution of the proposed concentration profiles (*dotted lines*) with the PSF experimentally measured in (*A*). (*B*) Fluorescence intensity profile of Survanta on a buffered-saline subphase. (*C*) Fluorescence intensity profile of albumin in a buffered-saline subphase. (*D*) Fluorescence intensity profile of either chitosan or PEG in a buffered-saline subphase. Profiles were calculated from z-stacks acquired at a surface pressure of 35 mN/m (*B*) or a fixed trough surface area of 115 cm^2 (*C* and *D*). Negative axial locations represent the air, positive locations correspond to the aqueous subphase, and the air-liquid interface is at zero.

profile was consistent with x-ray reflectivity measurements showing a densely packed layer of albumin alongside a less dense second layer with an approximate total thickness of 10 nm at the air-liquid interface (27). Both chitosan and PEG showed sigmoidal fluorescence intensity profiles with no interfacial peak (Fig. 3 *D*), corresponding to a step change in concentration at the interface with no surface activity. Adding either chitosan or PEG to the subphase did not significantly change the surface pressure, consistent with the lack of surface activity.

Although PEG and chitosan had identical axial distributions with no albumin or Survanta present, their distributions were distinctly different during inhibition reversal with albumin and Survanta also in the Langmuir trough. The sigmoidal fluorescence intensity profile of chitosan changed considerably in the presence of an interfacial film of albumin (Fig. 4 *A*). The chitosan profile almost identically matched that of albumin, including a peak in fluorescence intensity at the air-liquid interface. Chitosan likely adsorbed to albumin both at the interface and in the bulk, and neutralized the negative charges on the albumin. Addition of Survanta to the trough caused the albumin fluorescence intensity profile to change to a sigmoidal shape (Fig. 4 *B*), which was consistent with a constant bulk concentration of albumin and no surface activity. Using fluorescently labeled Survanta, we were able to observe that Survanta quantitatively replaced the albumin at the interface (Fig. 4 *C*). Chitosan remained at the interface with the anionic Survanta film during this replacement process.

The axial fluorescence profile of PEG remained sigmoidal, consistent with a constant subphase concentration and no surface activity, regardless of the presence of albumin or Survanta. With no Survanta present, PEG did not significantly affect the distribution of albumin (Fig. 4 *D*). However, the addition of Survanta to the subphase with PEG and albumin (Fig. 4 *E*) changed the albumin fluorescence profile dramatically from a peak at the interface to a sigmoidal profile, as was the case with chitosan under similar conditions (Fig. 4 *B*). Again, Survanta quantitatively replaced albumin at the air-liquid interface (Fig. 4 *F*). The exchange of albumin with Survanta at the interface did not alter the sigmoidal axial fluorescence distribution of PEG, which indicated PEG was uniformly distributed throughout the subphase as necessary for the depletion-attraction mechanism.

Lateral distributions of chitosan and PEG

We investigated the contrasting lateral distributions of chitosan and PEG interacting with an interfacial Survanta film. LS films are not laterally homogeneous, and instead form domains in which the anionic lipids become segregated

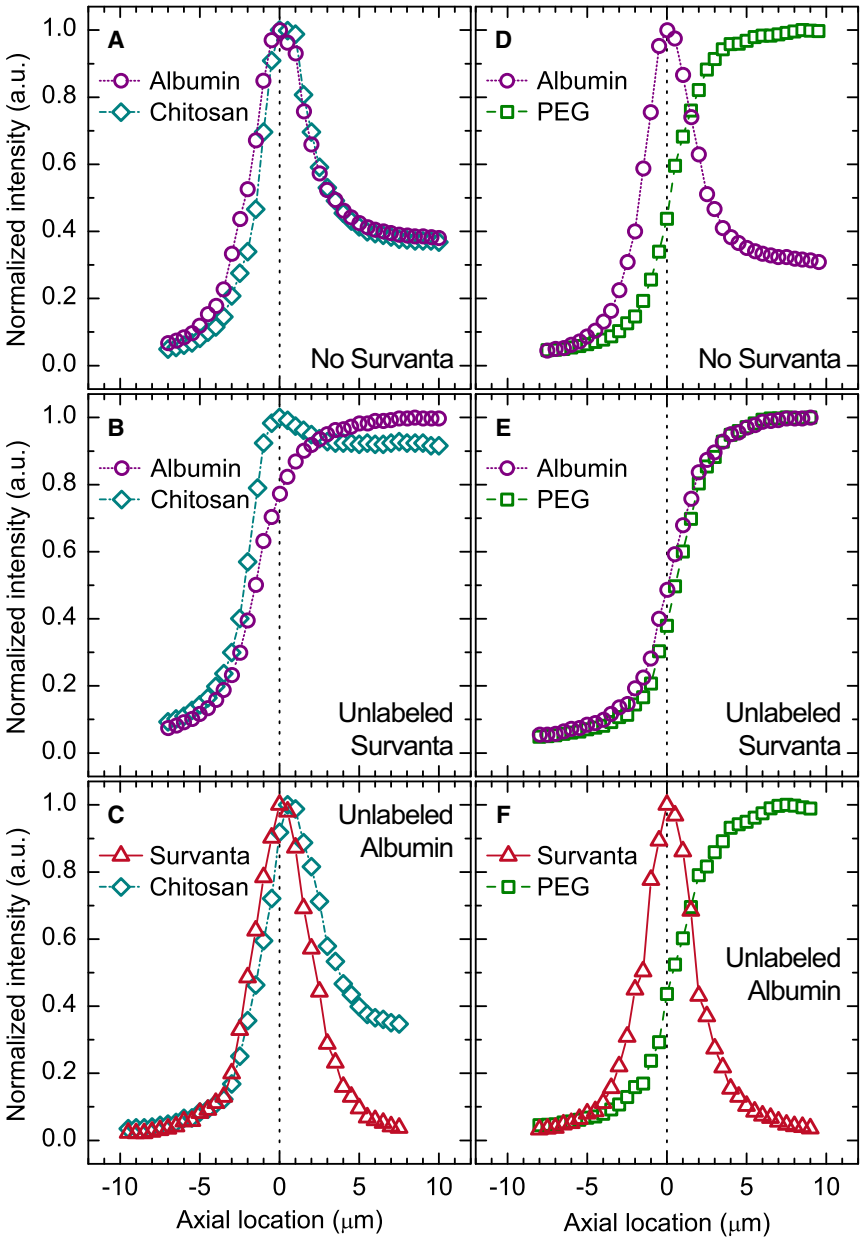

FIGURE 4 Effects of albumin and Survanta on the axial distributions of chitosan and PEG. (*A* and *B*) Axial profiles of albumin and chitosan in a buffered-saline subphase before (*A*) and after (*B*) the addition of unlabeled Survanta. (*C*) Survanta on a buffered-saline subphase containing chitosan and unlabeled albumin. (*D* and *E*) Albumin and PEG in a buffered-saline subphase before (*D*) and after (*E*) the addition of unlabeled Survanta. (*F*) Survanta on a buffered-saline subphase containing PEG and unlabeled albumin. Profiles were calculated from z-stacks acquired at a surface pressure of 35 mN/m (*B*, *E*, and *F*), a surface pressure of 30 mN/m (*C*), or a fixed trough surface area of 115 cm^2 (*A* and *D*). Negative axial locations represent the air, positive locations correspond to the aqueous subphase, and the air-liquid interface is at zero.

(34,36,37). The shallow depth-of-field of the confocal microscope resulted in a sharp delineation of the lateral distribution of Survanta, chitosan, and PEG at the interface. Survanta (Fig. 5 *A*) exhibited a characteristic mottled morphology consisting of bright domains of a less ordered, liquid-expanded (LE) phase in a continuous network of dark, more ordered, liquid-condensed (LC) phase (27,34,36,37). Contrast in the images resulted from the exclusion of the fluorescent lipid used to label Survanta from the semicrystalline LC phase and its inclusion in the LE phase (27,34,36,37), similar to one or two component lipid monolayers (38). No lateral variations were observed for either chitosan (Fig. 5 *B*) or PEG (Fig. 5 *C*) alone in the saline subphase.

In similarity to the axial distributions, the lateral distribution of chitosan correlated strongly with the domains in the Survanta film, whereas PEG remained homogeneously distributed at the interface. High concentrations of chitosan at the interface, indicated by the bright green regions (Fig. 5 *E*), strongly correlated with the bright red LE domains of Survanta (Fig. 5 *D*). The domains appeared bright yellow in the combined image showing a high degree of colocalization (Fig. 5 *F*). The observed association of the polycationic chitosan with the LE, red phase of Survanta confirmed earlier speculation that the anionic lipids in Survanta primarily segregate into the LE phase (34,36,37). The majority of anionic lipids in LS are unsaturated

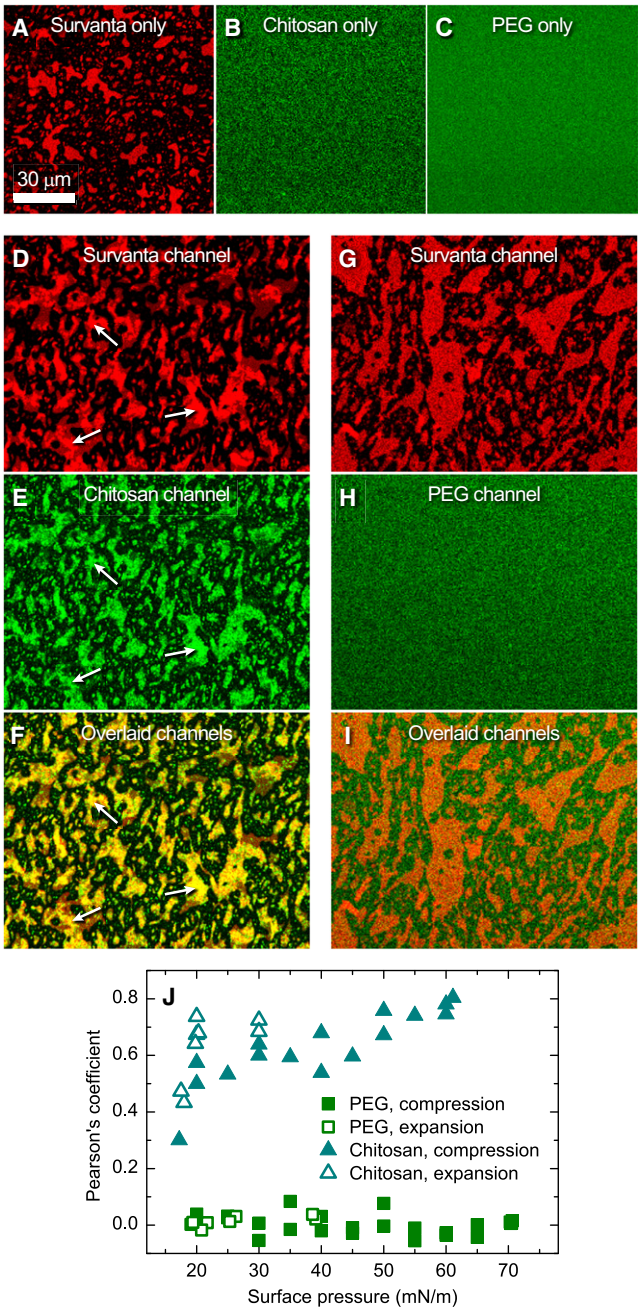

FIGURE 5 Lateral distribution of chitosan and PEG in relation to the anionic domains of Survanta. (*A–C*) Individual materials in the Langmuir trough with a buffered-saline subphase containing Survanta (*A*), chitosan (*B*), or PEG (*C*). (*D–F*) Simultaneous visualization of red (Survanta) and green (chitosan) fluorescence during inhibition reversal with Survanta on a buffered-saline subphase containing chitosan and unlabeled albumin. The mottled bright domains in a dark, continuous background in the Survanta images resulted from lateral phase separation into a dye-rich, LE phase and a dye-poor, LC phase, with the anionic lipids in Survanta concentrated in the LE domains. Brighter red, multilayered regions within the Survanta LE domains correlated most strongly with the brightest green domains of chitosan to give the brightest yellow regions in the overlaid image (*arrows*). (*G–I*) Simultaneous visualization of red (Survanta) and green (PEG) fluorescence during inhibition reversal with Survanta on a buffered-saline subphase containing PEG and unlabeled albumin. PEG showed no lateral structure or colocalization with the features of Survanta. (*J*) Pearson's colocalization coefficient, calculated using Eq. 3, as a function of surface pressure for multiple trough compression-expansion cycles. The scale bar in *A* applies to all images, which are displayed in a multichannel pseudocoloring scheme. The images were acquired at a surface pressure of 35 mN/m (*A* and *D–I*) or a fixed trough surface area of 115 cm^2 (*B* and *C*).

phosphatidylglycerols (39). In general, unsaturated lipids partition into the less-ordered LE phase (27,38,40). The semicrystalline LC phase contains more of the saturated phosphatidylcholine and fatty acids of Survanta (27,41). In contrast to chitosan, there was no apparent interaction between PEG and Survanta as PEG was uniformly laterally distributed in the presence of an interfacial Survanta film (Fig. 5, *G–I*). The colocalization of chitosan with the Survanta domains that contained the majority of the anionic lipids, in contrast to the uniform lateral distribution of PEG, indicates that chitosan neutralized the negatively charged portions of the surfactant film whereas PEG induced a depletion-attraction force.

Chitosan and PEG both increased the average size of the LE domains in the Survanta film (compare Fig. 5 *A* to Fig. 5, *D* and *G*) with PEG causing a much larger size increase. PEG may have induced the LE domains to coalesce and increase in size through a lateral depletion-attraction force resulting from the dehydration of the lipid headgroups (42,43). In contrast, chitosan likely neutralized the anionic lipids within the LE domains, which decreased the dipole density difference between the LE domains and continuous LC phase. As a result, the energy of the LE domains decreased, which led to an increase in the average domain size (38,44).

Colocalization as a function of surface pressure

The Pearson's colocalization coefficient (Eq. 3) was used to quantify the overlap between the LE domains of Survanta and either chitosan or PEG (Fig. 5 *J*). A value of +1 meant that the variance in the distribution of one color (e.g., chitosan) correlated perfectly with the variance in the distribution of another color (e.g., Survanta). A value of zero meant that the variance in the distribution of one color (e.g., PEG) did not correlate with the variance in the distribution of another color (e.g., Survanta). As expected from the lateral images at the air-liquid interface, the Pearson's colocalization coefficient between PEG and Survanta was independent of surface pressure and near zero in value. The lateral distribution of PEG, like the axial distribution, was not altered by the presence of albumin or Survanta at any point in the compression-expansion cycle. However, the Pearson's coefficient between chitosan and Survanta increased with surface pressure. The area per molecule in the monolayer decreased with increasing surface pressure, which increased the lateral density of the anionic lipids in the LE domains. At higher surface pressures, the LE phase was squeezed out into multilayers (34). In the lateral images, the less intensely colored

areas corresponded to the LE monolayer domains, and the brighter red areas highlighted by the arrows corresponded to multilayer patches directly attached to the interface below the LE domains (Fig. 5, *D–F*). A combination of the Survanta and chitosan channels (Fig. 5 *F*) showed that the areas of strongest colocalization (i.e., brightest yellow) corresponded to the brightest red regions of the Survanta film. Upon expansion of the film, the colocalization coefficient remained high until a surface pressure of ~20 mN/m was reached, at which point the coefficient dropped back to the value seen during compression (Fig. 5 *J*). We also observed this critical respreading pressure in the isotherms (Fig. 2 *C*) where the expansion curve flattened at ~20 mN/m, which corresponded to Survanta multilayers starting to reincorporate into the monolayer (7).

DISCUSSION

Our comparison of compression-expansion isotherms shows a distinct difference between films of albumin and Survanta at the interface (Fig. 2 *A*). Albumin behaves in a typical manner for a soluble surfactant, in that its surface pressure at a given subphase concentration remains relatively constant regardless of the surface compression (7). In contrast, the surface pressure of the insoluble Survanta increases with compression until the film collapses at a much higher surface pressure (34). With both albumin and Survanta in the Langmuir trough, the isotherm resembles that of albumin only, which suggests that Survanta does not reach the interface within an hour (9,13,27). However, because the surface pressure, Π, is the negative derivative of the Gibbs free energy, G, with respect to the interfacial area, A, at constant temperature, T: $\Pi = -(\partial G/\partial A)_T$, the higher-surface-pressure Survanta should always displace the lower-surface-pressure albumin at equilibrium. When albumin occupies the air-liquid interface, Survanta in the Langmuir trough clearly has no effect on the surface pressure (Fig. 2 *A*), even with expansion and contraction of the interface (7,9,13,27). This albumin-inhibited adsorption of Survanta can also be visualized with three-dimensional imaging of the air-liquid interface (see Fig. S1 in the Supporting Material). In the lung, the time per breath is on the order of seconds, so the hours-long delay of surfactant adsorption to the interface would effectively prevent LS from minimizing the work of breathing, which is consistent with the surfactant inactivation associated with ARDS (4,5).

In the lungs of an ARDS patient, and similarly in the Langmuir trough, abnormally high concentrations (2,5,6) of fast-diffusing albumin rapidly saturate the alveolar air-liquid interface, especially as new interface is generated during the lung expansion of inhalation (8). The normally spontaneous adsorption of Survanta slows because albumin creates an electrostatic barrier to the diffusion of Survanta to the interface (Fig. 1 *A*). In the presence of an energy barrier, the stability ratio, W, compares the actual flux of Survanta to the surface, J, with the uninhibited, diffusion-limited flux, J_0, and is proportional to the exponential of the maximum, Φ_{max}, of the DLVO potential (Eq. 1) (9,14,18,22):

$$W = \frac{J_0}{J} \propto \exp\left(\frac{\Phi_{max}}{kT}\right). \quad (4)$$

Decreasing Φ_{max} restores equilibrium regardless of whether that equilibrium results in the aggregation of colloids or the exchange of albumin with Survanta at an interface.

To reduce Φ_{max} and restore surfactant adsorption, we employed two common colloid flocculants: a polyelectrolyte (i.e., chitosan) (24) of opposite charge to Survanta and albumin, and a nonadsorbing polymer (i.e., PEG) (31). The axial fluorescence intensity profiles (Fig. 4) demonstrate that the highly cationic chitosan adsorbs strongly to both the negatively charged surfactant and albumin, neutralizing the surface charge, σ, and hence decreasing the magnitude of the surface potential, ψ_s (Eq.1; the bulk concentration of chitosan also reduces the Debye length, κ^{-1}) (23,24). This decreases Φ_{max} and enhances surfactant diffusion to the interface, which leads to a much faster equilibrium exchange of albumin with Survanta at the air-liquid interface (Figs. 4 and 5).

The subphase pH substantially affects (Eq. 1) the optimum chitosan concentration for Survanta adsorption. Previous researchers observed an optimal chitosan concentration of 1–5 μg/mL at pH 5.5 (21). Here, we investigated the effectiveness of chitosan at pH 6.9 to better represent physiological conditions, and found that the optimum chitosan concentration increased to 25–50 μg/mL (Fig. 2 *B*). At pH 5.5, the net charge on albumin is -3, and the cationic groups on chitosan are ~90% dissociated (15,23,45). However, the net charge on albumin increases to -8, whereas chitosan is only ~30% dissociated at pH 6.9 (15,23,45). For Survanta, the anionic lipids are primarily phosphatidylglycerols with a pK_a of 2.9 (46). Therefore, the surface charge of Survanta does not change appreciably as pH increases from 5.5 to 6.9. The increased negative charge of albumin suggests an equivalent increase in σ and ψ_s (Eq. 1). Furthermore, the decreased positive charge of chitosan means that charge neutralization requires an eightfold higher chitosan concentration at pH 6.9 than at pH 5.5. Additionally, the decreased chitosan charge density at higher pH also lowers the flocculation efficiency. A suspension of charged latex colloids required ~30% more chitosan to flocculate compared with the amount calculated by stoichiometric charge neutralization when the chitosan charge density was similarly decreased (23). All of these estimates predict a 10-fold increase in optimum chitosan concentration at pH 6.9 compared with pH 5.5, which agrees well with the observed increase.

Neutral and nonadsorbing PEG does not alter the electrostatic interaction between Survanta and albumin, but instead generates a depletion-attraction potential (Eq. 2) that lowers

Φ_{max} (Eq. 4) and promotes the equilibrium exchange of albumin with Survanta at the interface. PEG induces an unbalanced osmotic pressure on the Survanta particles that enhances Survanta adsorption. Intrinsic to the depletion-attraction mechanism is the lack of interaction between PEG and either Survanta, albumin, or the interface. If PEG adsorbed to the interface, to albumin, or to Survanta, there would be no decrease in concentration in the gaps between surfactant particles and the interface, and therefore no depletion attraction. PEG remained uniformly distributed in solution during the exchange of albumin with Survanta at the interface (Figs. 4 and 5), which is consistent with the assumed nonadsorbing behavior of PEG that allows it to induce a depletion-attraction potential. To the best of our knowledge, this is the first visualization of these fundamental features of the depletion attraction.

Although PEG and chitosan operate through two distinctly different mechanisms, the axial fluorescence intensity profiles show that they both allowed for quantitative replacement of the low-surface-pressure albumin film with a higher-surface-pressure Survanta film, as expected from equilibrium thermodynamics. It has been suggested that albumin coexists with interfacial films of surfactant (when cospread at the air-liquid interface) to surface pressures well beyond the equilibrium surface pressure of albumin, and that this coexistence may be another mode of surfactant inactivation during ARDS (47). Although this may be an intermediate step in the exchange of albumin with Survanta (27), especially at surface pressures < 25 mN/m, our results are not consistent with albumin and Survanta coexisting or mixing at the interface. At surface pressures > 30 mN/m, the fluorescence intensity due to albumin at the interface disappeared, and the albumin profile was consistent with that of a uniform subphase concentration (compare Fig. 4, *A* and *D*, to Fig. 4, *B* and *E*).

Direct visualization of Survanta adsorption in the presence of albumin demonstrates the close analogy between colloid stability and the competitive adsorption of LS and serum proteins. The same additives used to flocculate colloids enhanced LS adsorption to the interface and promoted a thermodynamically preferred exchange of the inhibitory albumin film with LS. Using confocal microscopy, we demonstrated that the three-dimensional distributions of chitosan and PEG were consistent with two distinct mechanisms: a charge neutralization mechanism for chitosan, and a depletion-attraction mechanism for PEG. Although chitosan was not surface-active by itself, it coadsorbed with interfacial films of both Survanta and albumin, colocalized with the anionic lipids in the Survanta film, and also led to the quantitative exchange of albumin with Survanta at the interface. The optimum concentration of chitosan was pH-sensitive and determined by the degree of dissociation (i.e., net charge) of chitosan, albumin, and Survanta. In contrast, the distribution of PEG remained unchanged in the presence of Survanta or albumin, although the induced depletion-attraction force quantitatively exchanged albumin with Survanta at the interface. Overall, these results can be applied when competitive adsorption must be controlled to reverse a kinetically hindered equilibrium. Finally, we should use our understanding of colloid stability when engineering surfactant additives to promote inhibition reversal in ARDS.

SUPPORTING MATERIAL

A figure is available at http://www.biophysj.org/biophysj/supplemental/S0006-3495(12)00087-2.

We gratefully acknowledge helpful discussions with H. W. Taeusch, who started us on these investigations of surfactant inhibition, as well as financial support from National Institutes of Health (NIH) grant HL-51177. A.J.W. was also supported by NIH grants ES-015330 and HL-092158.

REFERENCES

1. Clements, J. A., and M. E. Avery. 1998. Lung surfactant and neonatal respiratory distress syndrome. *Am. J. Respir. Crit. Care Med.* 157:S59–S66.
2. Ware, L. B., and M. A. Matthay. 2000. The acute respiratory distress syndrome. *N. Engl. J. Med.* 342:1334–1349.
3. Zambon, M., and J. L. Vincent. 2008. Mortality rates for patients with acute lung injury/ARDS have decreased over time. *Chest.* 133:1120–1127.
4. Zuo, Y. Y., R. A. W. Veldhuizen, …, F. Possmayer. 2008. Current perspectives in pulmonary surfactant-inhibition, enhancement and evaluation. *Biochim. Biophys. Acta Biomembr.* 1778:1947–1977.
5. Da Silva, K., L. A. McCaig, …, F. Possmayer. 2005. Protein inhibition of surfactant during mechanical ventilation of isolated rat lungs. *Exp. Lung Res.* 31:745–758.
6. Ishizaka, A., T. Matsuda, …, S. Hashimoto. 2004. Elevation of KL-6, a lung epithelial cell marker, in plasma and epithelial lining fluid in acute respiratory distress syndrome. *Am. J. Physiol. Lung Cell. Mol. Physiol.* 286:L1088–L1094.
7. Warriner, H. E., J. Ding, …, J. A. Zasadzinski. 2002. A concentration-dependent mechanism by which serum albumin inactivates replacement lung surfactants. *Biophys. J.* 82:835–842.
8. Taeusch, H. W., J. Bernardino de la Serna, …, J. A. Zasadzinski. 2005. Inactivation of pulmonary surfactant due to serum-inhibited adsorption and reversal by hydrophilic polymers: experimental. *Biophys. J.* 89:1769–1779.
9. Zasadzinski, J. A., P. C. Stenger, …, P. Dhar. 2010. Overcoming rapid inactivation of lung surfactant: analogies between competitive adsorption and colloid stability. *Biochim. Biophys. Acta Biomembr.* 1798:801–828.
10. Holm, B. A., G. Enhorning, and R. H. Notter. 1988. A biophysical mechanism by which plasma proteins inhibit lung surfactant activity. *Chem. Phys. Lipids.* 49:49–55.
11. Krishnan, A., J. Sturgeon, …, E. A. Vogler. 2004. Scaled interfacial activity of proteins at the liquid-vapor interface. *J. Biomed. Mater. Res. A.* 68:544–557.
12. Pocivavsek, L., S. L. Frey, …, K. Y. Lee. 2008. Lateral stress relaxation and collapse in lipid monolayers. *Soft Matter.* 4:2019–2029.
13. Stenger, P. C., and J. A. Zasadzinski. 2007. Enhanced surfactant adsorption via polymer depletion forces: a simple model for reversing surfactant inhibition in acute respiratory distress syndrome. *Biophys. J.* 92:3–9.

14. Zasadzinski, J. A., T. F. Alig, …, H. W. Taeusch. 2005. Inhibition of pulmonary surfactant adsorption by serum and the mechanisms of reversal by hydrophilic polymers: theory. *Biophys. J.* 89:1621–1629.

15. Böhme, U., and U. Scheler. 2007. Effective charge of bovine serum albumin determined by electrophoresis NMR. *Chem. Phys. Lett.* 435:342–345.

16. Derjaguin, B. V., and L. Landau. 1941. Theory of the stability of strongly charged lyophobic sols and the adhesion of strongly charged particles in solutions of electrolytes. *Acta Physicochim. URSS.* 14:633–662.

17. Verwey, E. J. W., and J. T. G. Overbeek. 1948. Theory of the Stability of Lyophobic Colloids, 1st ed. Elsevier, New York.

18. Stenger, P. C., S. G. Isbell, …, J. A. Zasadzinski. 2009. Rediscovering the Schulze-Hardy rule in competitive adsorption to an air-water interface. *Langmuir.* 25:10045–10050.

19. Blanco, O., and J. Pérez-Gil. 2007. Biochemical and pharmacological differences between preparations of exogenous natural surfactant used to treat respiratory distress syndrome: role of the different components in an efficient pulmonary surfactant. *Eur. J. Pharmacol.* 568:1–15.

20. Zuo, Y. Y., H. Alolabi, …, A. W. Neumann. 2006. Chitosan enhances the in vitro surface activity of dilute lung surfactant preparations and resists albumin-induced inactivation. *Pediatr. Res.* 60:125–130.

21. Stenger, P. C., O. A. Palazoglu, and J. A. Zasadzinski. 2009. Mechanisms of polyelectrolyte enhanced surfactant adsorption at the air-water interface. *Biochim. Biophys. Acta Biomembr.* 1788:1033–1043.

22. Hunter, R. J. 1986. Foundations of Colloid Science, 1st ed. Oxford University Press, New York.

23. Ashmore, M., and J. Hearn. 2000. Flocculation of model latex particles by chitosans of varying degrees of acetylation. *Langmuir.* 16:4906–4911.

24. Bouyer, F., A. Robben, …, M. Borkovec. 2001. Aggregation of colloidal particles in the presence of oppositely charged polyelectrolytes: effect of surface charge heterogeneities. *Langmuir.* 17:5225–5231.

25. Lu, J. J., W. W. Y. Cheung, …, A. W. Neumann. 2002. The effect of dextran to restore the activity of pulmonary surfactant inhibited by albumin. *Respir. Physiol. Neurobiol.* 130:169–179.

26. Stenger, P. C., S. G. Isbell, and J. A. Zasadzinski. 2008. Molecular weight dependence of the depletion attraction and its effects on the competitive adsorption of lung surfactant. *Biochim. Biophys. Acta Biomembr.* 1778:2032–2040.

27. Stenger, P. C., G. Wu, …, J. A. Zasadzinski. 2009. X-ray diffraction and reflectivity validation of the depletion attraction in the competitive adsorption of lung surfactant and albumin. *Biophys. J.* 97:777–786.

28. Taeusch, H. W., K. W. Lu, …, J. A. Clements. 1999. Nonionic polymers reverse inactivation of surfactant by meconium and other substances. *Am. J. Respir. Crit. Care Med.* 159:1391–1395.

29. Lu, K. W., H. W. Taeusch, …, J. A. Clements. 2001. Polyethylene glycol/surfactant mixtures improve lung function after HCl and endotoxin lung injuries. *Am. J. Respir. Crit. Care Med.* 164:1531–1536.

30. Kobayashi, T., K. Ohta, …, K. Yamamoto. 1999. Dextran restores albumin-inhibited surface activity of pulmonary surfactant extract. *J. Appl. Physiol.* 86:1778–1784.

31. Asakura, S., and F. Oosawa. 1958. Interaction between particles suspended in solutions of macromolecules. *J. Polym. Sci.* 33:183–192.

32. Kaplan, P. D., J. L. Rouke, …, D. J. Pine. 1994. Entropically driven surface phase separation in binary colloidal mixtures. *Phys. Rev. Lett.* 72:582–585.

33. Banks, P. R., and D. M. Paquette. 1995. Comparison of three common amine reactive fluorescent probes used for conjugation to biomolecules by capillary zone electrophoresis. *Bioconjug. Chem.* 6:447–458.

34. Alonso, C., T. F. Alig, …, J. A. Zasadzinski. 2004. More than a monolayer: relating lung surfactant structure and mechanics to composition. *Biophys. J.* 87:4188–4202.

35. Pawley, J. B. 2006. Handbook of Biological Confocal Microscopy, 3rd ed. Springer, New York.

36. Ding, J., I. Doudevski, …, M. A. Sherman. 2003. Nanostructure changes in lung surfactant monolayers induced by interactions between palmitoyloleoylphosphatidylglycerol and surfactant protein B. *Langmuir.* 19:1539–1550.

37. Takamoto, D. Y., M. M. Lipp, …, J. A. Zasadzinski. 2001. Interaction of lung surfactant proteins with anionic phospholipids. *Biophys. J.* 81:153–169.

38. McConnell, H. M. 1991. Structures and transitions in lipid monolayers at the air-water interface. *Annu. Rev. Phys. Chem.* 42:171–195.

39. Bernhard, W., J. Mottaghian, …, C. F. Poets. 2000. Commercial versus native surfactants: surface activity, molecular components, and the effect of calcium. *Am. J. Respir. Crit. Care Med.* 162:1524–1533.

40. Veatch, S. L., and S. L. Keller. 2005. Seeing spots: complex phase behavior in simple membranes. *Biochim. Biophys. Acta Biomembr.* 1746:172–185.

41. Bringezu, F., J. Ding, …, J. A. Zasadzinski. 2001. Changes in model lung surfactant monolayers induced by palmitic acid. *Langmuir.* 17:4641–4648.

42. Safran, S. A., T. L. Kuhl, and J. N. Israelachvili. 2001. Polymer-induced membrane contraction, phase separation, and fusion via Marangoni flow. *Biophys. J.* 81:659–666.

43. Lehtonen, J. Y. A., and P. K. J. Kinnunen. 1995. Poly(ethylene glycol)-induced and temperature-dependent phase separation in fluid binary phospholipid membranes. *Biophys. J.* 68:525–535.

44. Lee, D. W., Y. Min, …, J. A. Zasadzinski. 2011. Relating domain size distribution to line tension and molecular dipole density in model cytoplasmic myelin lipid monolayers. *Proc. Natl. Acad. Sci. USA.* 108:9425–9430.

45. Domard, A. 1987. pH and C.D. measurements on a fully deacetylated chitosan: application to Cu(II)-polymer interactions. *Int. J. Biol. Macromol.* 9:98–104.

46. Watts, A., K. Harlos, …, D. Marsh. 1978. Control of the structure and fluidity of phosphatidylglycerol bilayers by pH titration. *Biochim. Biophys. Acta Biomembr.* 510:63–74.

47. Zuo, Y. Y., S. M. Tadayyon, …, F. Possmayer. 2008. Atomic force microscopy studies of functional and dysfunctional pulmonary surfactant films, II: albumin-inhibited pulmonary surfactant films and the effect of SP-A. *Biophys. J.* 95:2779–2791.